AIMS Mathematics, 11(8): 26868–26896.
DOI: 10.3934/math.20261078
Received: 17 June 2026
Revised: 31 July 2026
Accepted: 11 August 2026
Published: 26 August 2026

https://www.aimspress.com/journal/Math

Research article

Complex population patterns in a discrete-time predator-prey model incorporating fear and harvesting and chaos control

Figen Kangalgil[1], **Nilüfer Topsakal**[2] **and Mehmet Unlu**[3,*]

[1] Bergama Vocational School, Dokuz Eylul University, 35700 Bergama, Izmir, Türkiye
[2] Department of Mathematics, Sivas Cumhuriyet University, 58140 Sivas, Türkiye
[3] Department of Mathematics, Recep Tayyip Erdogan University, 53100 Rize, Türkiye

* **Correspondence:** Email: mehmet.unlu@erdogan.edu.tr.

Abstract: This study examines the effects of incorporating harvesting and fear effects into a discrete-time predator-prey amensalism population model on system dynamics. To establish a more realistic ecological model framework, the study considers not only classical predator-prey interactions, but also the behavioral responses of prey individuals to the presence of predators and human-induced external interventions. The model was analyzed using mathematical methods and detailed numerical simulations; additionally, bifurcation analysis was performed. The existence and local stability of all equilibrium points have been determined, and a topological classification of these points has been performed. Obtained results indicate that an increase in fear and hunting levels reduces prey population density in the stable region, whereas it has no significant effect on the predator population. Furthermore, it was demonstrated that the system undergoes a flip (period-doubling) bifurcation, which can lead to complex or even chaotic dynamics. An Ott-Grebogi-Yorke (OGY) feedback control strategy was applied to control erratic behavior, and it was shown that this method is effective in stabilizing unstable periodic orbits. Overall, this study explains how fear-induced behavioral responses and the harvesting effect jointly influence prey and predator populations, providing important insights into the stabilization and management of discrete-time ecological systems.

Keywords: prey-predator; chaos; fear effect; harvesting effect; amensalism
Mathematics Subject Classification: 37D45, 37G35, 37N25, 39A30, 92D25, 93D15

1. Introduction

Predator-prey interactions form a cornerstone of theoretical ecology, providing essential insights into population dynamics and ecosystem stability. Classical frameworks, most notably the Lotka–Volterra equations, offer a fundamental tool for understanding these interactions and explain the

cyclical fluctuations of prey and predator populations under idealized conditions. In the Lotka–Volterra model, prey populations grow exponentially in the absence of predators, while predator populations decline when prey is unavailable, generating characteristic oscillatory dynamics driven by species interactions. Despite its simplicity, the model has been pivotal in highlighting key principles such as the existence of equilibrium points and the persistence of population cycles. Contemporary extensions of the Lotka–Volterra framework incorporate ecological realism by including factors such as resource limitations, environmental carrying capacities, fear-induced behavioral responses, and harvesting pressures. These enhancements enable researchers to investigate more complex dynamics, including bifurcations, chaotic behavior, and the stabilizing effects of behavioral adaptations or management strategies, thereby bridging the gap between theoretical predictions and empirical ecological patterns. Population dynamics are shaped by numerous biological and environmental factors, including fear responses, infectious diseases, stage structure, latency, harvesting, and other ecological pressures. Among these, predator-induced fear has attracted considerable attention because it can significantly suppress prey reproduction and alter population growth rates.

The impact of predator-induced fear on predator-prey dynamics has received considerable attention in recent mathematical ecology studies and has been investigated using various modeling frameworks. Ecologically, fear represents a major non-consumptive effect, influencing both the behavior and physiological processes of prey through stress-mediated responses. Even in the absence of direct predation, the perceived risk of predation can prompt prey populations to adjust essential life-history traits, including reproduction, foraging activity, and movement patterns. One of the earliest biological explanations for these stress-driven responses is provided by the classical "fight-or-flight" concept introduced by Cannon [1]. Motivated by these biological observations, numerous mathematical models have incorporated fear effects to better capture the indirect influence of predators. In particular, Wang et al. [2,3] developed one of the pioneering predator-prey models incorporating fear-induced reductions in prey reproduction and demonstrated that, under a bilinear functional response, fear does not affect the stability of the coexistence equilibrium, whereas under a Holling type II functional response it may contribute to system stabilization. These findings have inspired further investigations into how fear interacts with other ecological mechanisms. For example, Pijush et al. [4] analyzed the stability and bifurcation structure of a predator-prey model that simultaneously includes fear effects and cooperative harvesting, while Zhang et al. [5] showed that the combined presence of fear and prey refuge can enhance the stability of ecological systems. More broadly, mathematical modeling has proven to be an effective framework for understanding how fear-driven behavioral responses shape predator-prey interactions. Recent studies have incorporated multi-species food chains [6, 7], predator interference and group defense [8], hunting cooperation [9], time delays and anti-predator behaviors [10, 11], and stochastic effects with intraguild predation and predator switching [12].

Existing studies have demonstrated that fear effects can significantly influence predator-prey dynamics by altering prey reproduction and stability (e.g., Wang et al. [2]; Zhang et al. [5]), whereas harvesting has been shown to modify equilibrium structure, induce bifurcations, and generate complex dynamics (e.g., Dai and Tang [13]; Elmacı and Kangalgil [14]). More recently, Jamil and Naji [15] investigated the combined influence of fear and harvesting in a Leslie–Gower predator-prey model, while Chong et al. [16] analyzed the influence of fear on a continuous-time Lotka–Volterra amensalism model. In contrast to these studies, the present work develops and analyzes a discrete-time predator-prey amensalism model that simultaneously incorporates fear and harvesting effects. The discrete-time

formulation enables the investigation of flip bifurcation, chaotic dynamics, and Ott-Grebogi-Yorke (OGY) chaos control, thereby providing new insights into the nonlinear dynamics of amensalism systems that are not available in the corresponding continuous-time framework. Collectively, these contributions indicate that fear can substantially influence the qualitative dynamics of predator-prey systems, potentially leading to stabilization, bistability, or more complex bifurcation patterns depending on the ecological and structural assumptions of the model.

Harvesting constitutes another crucial factor shaping population dynamics. The extraction of biological resources-common in fisheries, forestry, and wildlife management-directly modifies growth trajectories and equilibrium densities. Classical studies on harvested predator-prey systems [13, 17, 18] demonstrated that harvesting can significantly reduce equilibrium population levels and alter coexistence conditions. More recent discrete-time investigations reveal that harvesting may induce bifurcations, multistability, and chaotic behavior [14, 19]. Importantly, harvesting introduces extinction risk even in populations that would otherwise persist in the absence of exploitation. The joint consideration of fear and harvesting effects has attracted increasing attention in ecological modeling [15,20]. Fear modifies reproductive output and interaction strength, while harvesting directly removes individuals, leading to potentially intricate dynamical outcomes.

Population dynamics are typically investigated using either discrete-time or continuous-time models. Discrete-time formulations, expressed through difference equations, are particularly effective for populations with non-overlapping generations, where changes unfold in distinct, sequential intervals. This approach not only reflects the inherent structure of such populations, but also corresponds closely to empirical data, which are frequently gathered at fixed time points, such as annually or seasonally. Beyond evaluating stability, discrete-time models provide a robust framework for exploring complex dynamics, including oscillatory and chaotic behaviors, which are often less apparent in continuous-time representations. Their capacity to capture subtle, nonlinear interactions within populations underscores the essential role of discrete-time modeling in ecological and biological research. By incorporating ecological mechanisms such as immigration, harvesting, and Allee effects, discrete-time models provide a versatile framework for investigating population dynamics [19, 21]. Their applications to predator-prey systems have also revealed complex dynamics, including bifurcations and chaos [22, 23].

Chaotic behavior occurs in numerous complex systems, including lasers, nonlinear optical setups, optimization processes, biological models, and chemical reactions. Nonlinear dynamical systems often display intricate behaviors that can induce significant qualitative changes in their steady-state trajectories, such as chaos, bifurcations, coexisting attractors, and fractal basin boundaries. Since these phenomena may lead to system instability or undesirable operation, effective control strategies are crucial. Various methods have been proposed for chaos suppression, including the OGY method, feedback linearization, cycle-to-cycle variable slope compensation, time-delayed feedback, and fuzzy control [24]. These techniques stabilize chaotic systems along unstable periodic orbits embedded within strange attractors using minimal perturbations. In this study, the OGY feedback control method is employed to suppress the observed chaotic dynamics.

Among the various ecological interactions between species, amensalism and commensalism are commonly observed in nature. Amensalism refers to an interaction in which one species is adversely affected by another species, while the latter experiences neither benefit nor harm. In contrast, commensalism describes a unidirectional relationship in which one species benefits and the other

remains unaffected. Although commensalism models have been extensively studied, including positive periodic solutions [25, 26], stability and attractivity [27–29], models incorporating harvesting and impulsive effects [30, 31], as well as various functional responses [32–34], amensalism models have received comparatively less attention. Existing studies have considered positive periodic solutions and qualitative properties [35–37], non-monotonic and Holling-type functional responses [38, 39], and the dynamic behavior and mathematical analysis of amensalism systems [40, 41]. The first two-species amensalism model was proposed by Sun [37] in the following form:

$$\begin{cases} \dfrac{dx}{dt} = r_1 x\left(\dfrac{k_1 - x - \alpha y}{k_1}\right), \\ \dfrac{dy}{dt} = r_2 y\left(\dfrac{k_2 - y}{k_2}\right). \end{cases} \tag{1.1}$$

The stability of all equilibria for the system is thoroughly analyzed. Furthermore, Zhu and Chen [41] examined the qualitative properties of a more general amensalism model, formulated as follows:

$$\begin{cases} \dfrac{dx}{dt} = x\left(b_1 - a_1 x - a_2 y\right), \\ \dfrac{dy}{dt} = y\left(b_2 - \alpha_3 y\right). \end{cases} \tag{1.2}$$

Recently, several studies have focused on how harvesting affects amensalism and commensalism systems [30, 42]. Therefore, the aim of this study is to investigate how harvest and fear influence the Lotka-Volterra amensalism model. To date, the influence of fear and harvesting within amensalism systems remains unexplored in academic literature. As noted by Xi, Griffin, and Sun [43], grassland caterpillars and grasshoppers represent two primary herbivorous insects in these ecosystems. Specifically, the unintentional disturbance caused by the natural jumping of grasshoppers severely disrupts the feeding patterns of caterpillars. This disruption retards their development rate and ultimately reduces the fecundity of female caterpillars. Consequently, the presence of grasshoppers profoundly alters caterpillar behavior and life history, encompassing their feeding habits, growth rates, survival, reproductive investments, and developmental timing. In essence, this grasshopper-induced fear leads to a decreased birth rate and an increased mortality rate among caterpillars. While formulating mathematical models to capture this phenomenon is essential, an amensalism model incorporating the fear effect has yet to be proposed. To address this gap, this paper establishes a Lotka-Volterra model that accounts for the fear and harvesting effects on the affected species, exploring its consequences on the dynamic behavior of the amensalism system.

We discretize system (1.2) and then add both the influence of harvesting and fear affecting. We consider the following discrete-time prey-predator amensalism model:

$$\begin{cases} x_{t+1} = x_t + \delta\left(\dfrac{x_t(b_1 - a_1\, x_t)}{1 + f\, y_t} - a_2\, x_t\, y_t - h\, x_t\right), \\ y_{t+1} = y_t + \delta\, y_t(b_2 - a_3\, y_t), \end{cases} \tag{1.3}$$

where h is the harvesting parameter, b_1 is growth rate of the species x, b_2 is growth rate of the species y, $\dfrac{b_1}{a_1}$, $\dfrac{b_2}{a_3}$ are the carrying capacity of species x and y, respectively, and a_2 reflects the efficiency of

every single population y that can contribute to population x. The quantity $\frac{1}{1+fy}$ describes the fear effect of the first species. Note that all parameters are positive constants. Moreover, here, $\delta > 0$ denotes the time-step (discretization parameter) obtained from the forward Euler discretization of the corresponding continuous-time model. Biologically, δ represents the time interval between two successive observations or updates of the population densities, while mathematically it controls the discretization of the continuous-time dynamics. Since the dynamical behavior of discrete-time systems may depend on the step size, δ is also treated as a bifurcation parameter in the subsequent analysis. The biological interpretations of the parameters appearing in system (1.3) are summarized in Table 1.

Table 1. Biological meaning of the parameters in system (1.3).

Parameter	Biological meaning of parameter
δ	Time-step discretization parameter
$\frac{b_1}{a_1}$	Carrying capacity of species x
a_2	Efficiency of every single population y that can contribute to population x
$\frac{b_2}{a_3}$	Carrying capacity of species y
b_1	Growth rate of the species x
b_2	Growth rate of the species y
h	Harvesting effect
f	Fear effect

The motivation for this study stems from the fact that fear effects and harvesting are two important ecological mechanisms that can substantially influence population dynamics, yet their combined impact on discrete-time predator-prey amensalism systems has received little attention. To the best of our knowledge, this study is one of the few to develop and analyze a discrete-time predator-prey amensalism model that simultaneously incorporates both fear and harvesting effects. The proposed model enables a comprehensive investigation of how these mechanisms jointly affect the existence and stability of equilibria, the emergence of flip bifurcation and chaotic dynamics, and the effectiveness of chaos control via the OGY method. These features distinguish the present work from existing predator-prey and amensalism models and constitute the principal novelty of the manuscript.

The choice of a discrete-time framework is motivated by both biological and mathematical considerations. Biologically, many populations, particularly insects, annual plants, and other seasonal species, reproduce in distinct breeding periods, making discrete-time models more appropriate than continuous-time formulations. In addition, ecological observations are often recorded at fixed sampling intervals, such as annually or seasonally, which naturally aligns with discrete-time modeling. From a dynamical perspective, discrete-time systems can exhibit rich nonlinear phenomena, including period-doubling bifurcations and chaotic dynamics, that are essential for understanding complex population behavior. Since one of the main objectives of this work is to investigate the occurrence of flip bifurcation and chaos in a predator-prey amensalism model with fear and harvesting effects, the discrete-time framework provides a natural and appropriate setting for the present analysis. Although the proposed model is derived from a continuous-time predator-prey amensalism framework, its

discrete-time formulation is not simply a numerical approximation. Instead, it constitutes a distinct dynamical system with qualitative properties that differ fundamentally from those of its continuous-time counterpart. In particular, discrete-time systems can exhibit flip bifurcations, complex oscillatory dynamics, and chaos through mechanisms that are absent or substantially different in continuous-time models. Consequently, the discrete-time formulation provides additional insight into the long-term behavior of ecological systems and enables the investigation of nonlinear phenomena that cannot be captured by the corresponding continuous-time model. These distinctive dynamical characteristics provide the primary motivation for adopting the discrete-time framework in the present study.

The main contributions of this study are summarized as follows, emphasizing the combined roles of fear and harvesting in shaping the dynamical behavior of the proposed discrete-time predator-prey system.

- Amensalism can be regarded as a special case of the Lotka–Volterra system with unidirectional interaction, where one species is affected by the other while the second species remains unaffected. This asymmetric interaction structure provides flexibility to the Lotka–Volterra framework, allowing it to be extended to include additional ecological effects such as harvesting and fear. Motivated by this structure, a new discrete-time predator-prey amensalism model is proposed by incorporating two important ecological factors: Fear, which reduces prey reproduction, and harvesting pressure. The proposed model captures both indirect behavioral responses and direct human-induced effects within a unified discrete-time framework.
- All equilibrium points of the system are determined, including the trivial equilibrium, boundary equilibria, and a unique positive interior equilibrium. Explicit parametric conditions guaranteeing the existence of the positive equilibrium are established.
- The local stability of each equilibrium point is analyzed using the Jacobian matrix and eigenvalue-based criteria. The analysis reveals that both fear intensity and harvesting rate play crucial roles in determining the stability regions of the system.
- It has been shown that an increase in the fear effect leads to a decrease in prey population density but does not result in a change in predator population density. Furthermore, an increase in fear intensity has accelerated the system's convergence to its equilibrium state.
- It has been observed that an increase in the harvesting effect reduces the density of prey populations and accelerates their approach to equilibrium. It has been observed that this effect does not influence the density of predator populations.
- By considering the step-size parameter as a bifurcation parameter, it is analytically and numerically demonstrated that the system undergoes a flip bifurcation at the positive equilibrium under specific conditions, marking the transition from stable equilibrium to oscillatory and potentially chaotic dynamics.
- Further variation of system parameters beyond the flip bifurcation leads to more complex dynamical behaviors, including chaotic dynamics, which are verified through bifurcation diagrams and Lyapunov exponent analysis.
- To control the chaotic behavior, the OGY feedback control method is implemented to stabilize the unstable equilibrium embedded within chaotic attractors. The controllability of the system is analytically verified and the admissible control region is identified.
- Extensive numerical simulations are carried out to support the theoretical findings, illustrating stability regions, bifurcation structures, chaotic dynamics, and the effectiveness of the proposed

chaos control strategy under biologically relevant parameter values.

2. Existence of the fixed points

In this section, we examine the existence of positive equilibrium points of system (1.3) and investigate their stability properties.

2.1. Invariant region

Lemma 2.1. *Let $x_0 > 0$ and $y_0 > 0$. Consider the discrete-time system*

$$x_{t+1} = x_t + \delta\left(\frac{x_t(b_1 - a_1x_t)}{1 + fy_t} - a_2x_ty_t - hx_t\right), \tag{2.1}$$

$$y_{t+1} = y_t + \delta y_t(b_2 - a_3y_t). \tag{2.2}$$

Then, the set

$$\mathcal{D} = \left\{(x, y) \in \mathbb{R}^2_+ \;\middle|\; 0 < y \leq \frac{b_2 + \frac{1}{\delta}}{a_3},\ 0 < x \leq \frac{b_1 - \left(a_2y + h - \frac{1}{\delta}\right)(1 + fy)}{a_1}\right\} \tag{2.3}$$

is positively invariant.

Proof. From the second equation, we write

$$y_{t+1} = y_t(1 + \delta(b_2 - a_3y_t)). \tag{2.4}$$

Since $y_t > 0$, the condition $y_{t+1} \geq 0$ holds if

$$1 + \delta(b_2 - a_3y_t) \geq 0, \tag{2.5}$$

which implies

$$y_t \leq \frac{b_2 + \frac{1}{\delta}}{a_3}. \tag{2.6}$$

Similarly, the first equation can be rewritten as

$$x_{t+1} = x_t\left[1 + \delta\left(\frac{b_1 - a_1x_t}{1 + fy_t} - a_2y_t - h\right)\right]. \tag{2.7}$$

For $x_t > 0$, the inequality $x_{t+1} \geq 0$ is satisfied whenever

$$1 + \delta\left(\frac{b_1 - a_1x_t}{1 + fy_t} - a_2y_t - h\right) \geq 0, \tag{2.8}$$

which yields

$$x_t \leq \frac{b_1 - \left(a_2y_t + h - \frac{1}{\delta}\right)(1 + fy_t)}{a_1}. \tag{2.9}$$

Hence, for any $(x_t, y_t) \in \mathcal{D}$, we have $x_{t+1} \geq 0$ and $y_{t+1} \geq 0$. Therefore, $\mathcal{D}$ is positively invariant. □

Definition 2.2. *A point* (x^*, y^*) *is said to be a fixed point (equilibrium point) of system* (1.3)*, if it satisfies*

$$\begin{cases} x^* = x^* + \delta\left(\dfrac{x^*(b_1 - a_1\, x^*)}{1 + f\, y^*} - a_2\, x^*\, y^* - h\, x^*\right), \\ y^* = y^* + \delta\, y^*(b_2 - a_3\, y^*). \end{cases} \tag{2.10}$$

Lemma 2.3. *The following statements hold:*

i) System (1.3) *always admits the trivial equilibrium* $E_1 = (0, 0)$.

ii) There exists a boundary equilibrium $E_2 = \left(\dfrac{b_1 - h}{a_1}, 0\right)$ *provided that* $b_1 > h$.

iii) Another boundary equilibrium is $E_3 = \left(0, \dfrac{b_2}{a_3}\right)$.

iv) The system possesses a unique positive interior equilibrium

$$E_4 = \left(\frac{a_3^2\, b_1 - (a_3 + b_2\, f)(a_2\, b_2 + a_3\, h)}{a_1\, a_3^2}, \frac{b_2}{a_3}\right),$$

whenever the condition $a_3^2\, b_1 > (a_3 + b_2\, f)(a_2\, b_2 + a_3\, h)$ *is satisfied.*

Next, we classify the equilibria of system (1.3) from a topological viewpoint. The Jacobian matrix evaluated at an arbitrary point (x, y) is given by

$$J(x, y) = \begin{bmatrix} 1 - h\delta - a_2\, y\, \delta + \dfrac{\delta(b_1 - 2a_1\, x)}{1 + f\, y} & -a_2\, x\, \delta + \dfrac{f\, x\, \delta(a_1\, x - b_1)}{(1 + f\, y)^2} \\ 0 & 1 + \delta\,(b_2 - 2a_3\, y) \end{bmatrix}. \tag{2.11}$$

The associated characteristic equation is

$$F(\lambda) = \lambda^2 - \mathrm{tr}[J(x, y)]\lambda + \det[J(x, y)] = 0, \tag{2.12}$$

where tr and det denote the trace and determinant of the Jacobian matrix, respectively.

Definition 2.4. Let λ_1 and λ_2 be the roots of the characteristic equation. Then, a fixed point of system (1.3) is classified as:

i) Sink if $|\lambda_1| < 1$ and $|\lambda_2| < 1$;
ii) Source if $|\lambda_1| > 1$ and $|\lambda_2| > 1$;
iii) Saddle if one eigenvalue lies inside the unit disk and the other lies outside, namely, $|\lambda_1| < 1$ and $|\lambda_2| > 1$ or $|\lambda_1| > 1$ and $|\lambda_2| < 1$;
iv) Nonhyperbolic if at least one eigenvalue satisfies $|\lambda_i| = 1$ where $i = 1, 2$.

We now evaluate the Jacobian matrix at each equilibrium point E_1, E_2, E_3, and E_4, respectively. For the trivial equilibrium $E_1 = (0, 0)$, the Jacobian matrix becomes

$$J(E_1) = \begin{bmatrix} 1 + \delta(b_1 - h) & 0 \\ 0 & 1 + b_2\, \delta \end{bmatrix}. \tag{2.13}$$

Thus, the eigenvalues are evaluated as

$$\lambda_1 = 1 + (b_1 - h)\delta, \qquad \lambda_2 = 1 + b_2\,\delta. \tag{2.14}$$

According to Definition 2.4, we can get the following lemma.

Lemma 2.5. *For the fixed point $E_1 = (0, 0)$, the following topological classification holds:*

i) The point E_1 is a source if $h > b_1$ and $\delta > \dfrac{2}{h - b_1}$ or $b_1 > h$;

ii) The point E_1 is a saddle if $h > b_1$ and $\delta < \dfrac{2}{h - b_1}$;

iii) The point E_1 is a nonhyperbolic if $\delta = \dfrac{2}{h - b_1}$.

The Jacobian matrix at the fixed point E_2 is obtained as

$$J(E_2) = \begin{bmatrix} 1 - \delta(b_1 - h) & -\dfrac{\delta(b_1 - h)(a_2 + f\,h)}{a_1} \\ 0 & 1 + b_2\,\delta \end{bmatrix}. \tag{2.15}$$

Thus, the eigenvalues are evaluated as

$$\lambda_1 = 1 - \delta(b_1 - h), \qquad \lambda_2 = 1 + b_2\,\delta. \tag{2.16}$$

Lemma 2.6. *For the fixed point $E_2 = \left(\dfrac{b_1 - h}{a_1}, 0\right)$, the following topological classification holds:*

i) The point E_2 is a source if $b_1 > h$ and $\delta > \dfrac{2}{b_1 - h}$;

ii) The point E_2 is a saddle if $b_1 > h$ and $\delta < \dfrac{2}{b_1 - h}$;

iii) The point E_2 is a nonhyperbolic if $\delta = \dfrac{2}{b_1 - h}$.

The Jacobian matrix at the fixed point E_3 is obtained as

$$J(E_3) = \begin{bmatrix} 1 + \delta\,\dfrac{a_3^2\,b_1 - (a_3 + b_2\,f)(a_2\,b_2 + a_3\,h)}{a_3(a_3 + b_2\,f)} & 0 \\ 0 & 1 - b_2\,\delta \end{bmatrix}. \tag{2.17}$$

Thus, the eigenvalues are evaluated as

$$\lambda_1 = 1 - b_2\,\delta, \qquad \lambda_2 = 1 + \delta(V_1 - V_2), \tag{2.18}$$

where we have defined

$$V_1 := \frac{a_3\,b_1}{a_3 + b_2\,f}, \qquad V_2 := \frac{a_2\,b_2 + a_3\,h}{a_3}. \tag{2.19}$$

Lemma 2.7. *For the fixed point $E_3 = \left(0, \dfrac{b_2}{a_3}\right)$, the following topological classification holds:*

i) The point E_3 is a sink if $\delta < min\Big\{\frac{2}{b_2}, \frac{2}{V_2 - V_1}\Big\}$ and $V_2 > V_1$.

ii) The point E_3 is a source if $\delta > max\Big\{\frac{2}{b_2}, \frac{2}{V_2 - V_1}\Big\}$ and $V_2 > V_1$ or $\delta > \frac{2}{b_2}$ and $V_2 < V_1$.

iii) The point E_3 is a saddle if $\delta < \frac{2}{b_2}, \delta > \frac{2}{V_2 - V_1}$, and $V_2 > V_1$; or $\delta < \frac{2}{b_2}$ and $V_2 < V_1$; or $\delta > \frac{2}{b_2}, \delta < \frac{2}{V_2 - V_1}$, and $V_2 > V_1$.

iv) The point E_3 is a nonhyperbolic if $\delta = \frac{2}{b_2}$; or $\delta = \frac{2}{V_2 - V_1}$ and $V_2 > V_1$; or $V_2 = V_1$.

The Jacobian matrix at the fixed point E_4 is obtained as

$$J(E_4) = \begin{bmatrix} j_{11} & j_{12} \\ j_{21} & j_{22} \end{bmatrix}, \tag{2.20}$$

where we have defined

$$j_{11} := 1 - \delta \frac{a_3^2 b_1 - (a_3 + b_2 f)(a_2 b_2 + a_3 h)}{a_3(a_3 + b_2 f)},$$

$$j_{12} := \frac{\delta(a_3 f h + a_3 a_2 + 2a_3 b_2 f)(-a_3^2 b_1 + (a_3 + b_2 f)(a_2 b_2 + a_3 h))}{a_1 a_3^2 (a_3 + b_2 f)},$$

$$j_{21} := 0, \qquad j_{22} := 1 - b_2 \delta.$$

Thus, the eigenvalues are evaluated as

$$\lambda_1 = 1 - b_2 \delta, \qquad \lambda_2 = 1 - \delta(V_1 - V_2), \tag{2.21}$$

where we recall that V_1 and V_2 are the quantities defined in (2.19).

Lemma 2.8. *For the fixed point E_4, the following topological classification holds:*

i) The point E_4 is a sink if $\delta < min\Big\{\frac{2}{b_2}, \frac{2}{V_1 - V_2}\Big\}$ and $V_1 > V_2$.

ii) The point E_4 is a source if $\delta > max\Big\{\frac{2}{b_2}, \frac{2}{V_1 - V_2}\Big\}$ and $V_1 > V_2$ or $\delta > \frac{2}{b_2}$ and $V_1 < V_2$.

iii) The point E_4 is a saddle if $\delta < \frac{2}{b_2}, \delta > \frac{2}{V_1 - V_2}$, and $V_1 > V_2$; or $\delta > \frac{2}{b_2}$ and $V_1 > V_2$; or $\delta > \frac{2}{b_2}$, $\delta < \frac{2}{V_1 - V_2}$ and $V_1 > V_2$.

iv) The point E_4 is a nonhyperbolic if $\delta = \frac{2}{b_2}$; or $\delta = \frac{2}{V_1 - V_2}$ and $V_1 = V_2$; or $V_1 = V_2$.

Example 2.1. *Using Lemma 2.8, we prove local asymptotical stability of model* (1.3)*. We take $a_1 = 1.7$, $a_2 = 0.4$, $a_3 = 0.5$, $b_1 = 9$, $b_2 = 5.5$, $f = 0.01, h = 0.8$, and initial condition $(x_0, y_0) = (1.8, 10.5)$, then the unique positive fixed point $E_4 = (0.4944950000, 1)$ is local asymptotically stable. The plots of x_n and y_n are shown in Figure 1.*

For $\delta \in (0.1, 1]$ and $h \in (0.1, 1]$, topological classification of the co-existence point is depicted in Figure 2, where the red region represents the sink, the blue region represents the source, and the green region represents saddle fixed points.

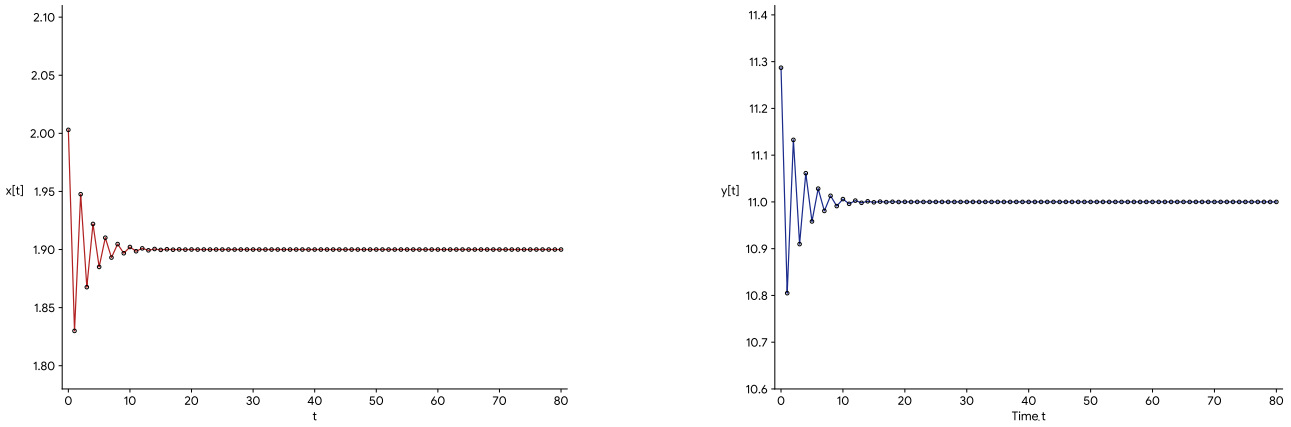

(a) **(b)**

Figure 1. Plots of the locally stable fixed point E_4 of system (1.3). The left panel shows the time series of x_t, while the right panel shows the time series of y_t.

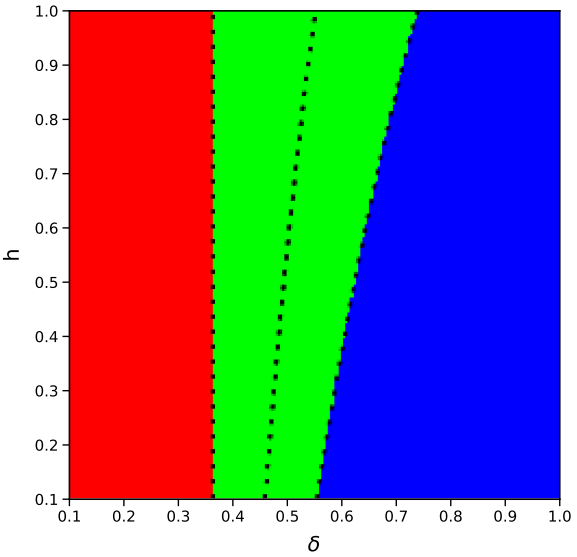

(a) Partition of the (δ, h)-parameter plane into regions with different topological classifications of the coexistence equilibrium point E_4.

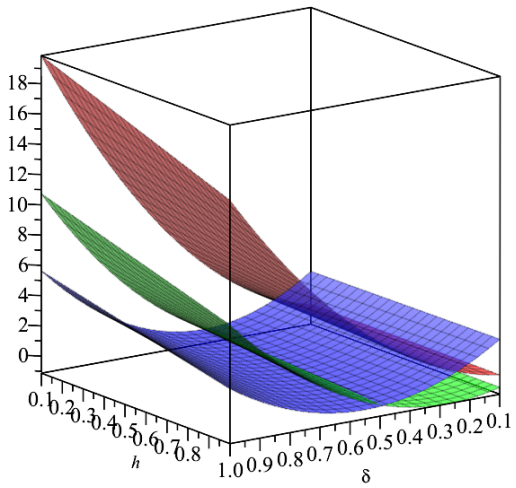

(b) Three-dimensional visualization of the characteristic surfaces associated with the topological classification of E_4 in the (δ, h)-parameter space.

Figure 2. Topological classification of the coexistence equilibrium point E_4 of system (1.3). Panel (a) shows the partition of the (δ, h)-parameter plane into regions corresponding to different qualitative behaviors, while panel (b) presents the corresponding characteristic surfaces that determine the boundaries between these regions.

3. Flip bifurcation analysis

Bifurcation theory plays an important role in understanding qualitative changes in the dynamics of nonlinear discrete systems as system parameters vary. In predator–prey models, small variations

in parameters may significantly influence the long-term population dynamics. Among the different bifurcation mechanisms observed in discrete dynamical systems, the flip bifurcation (also known as the period-doubling bifurcation) is particularly significant because it describes the transition from a stable equilibrium state to periodic oscillations.

Consider the discrete-time predator–prey system

$$X_{n+1} = F(X_n, p), \tag{3.1}$$

where $X = (x, y)$ denotes the prey and predator populations and p represents a bifurcation parameter. Let E^* be an equilibrium point of the system. The local stability of this equilibrium is determined by the eigenvalues of the Jacobian matrix evaluated at E^*.

Theorem 3.1. *Assume that the Jacobian matrix $J(E^*)$ evaluated at the equilibrium point E^* has eigenvalues λ_1 and λ_2. If there exists a parameter value $p = p^*$ such that*

$$\lambda_1 = -1, \qquad |\lambda_2| < 1, \tag{3.2}$$

and the corresponding nondegeneracy and transversality conditions are satisfied, then the discrete predator–prey system undergoes a flip bifurcation at the equilibrium point E^* when the parameter p passes through the critical value p^*. Consequently, a periodic orbit with period two bifurcates from the equilibrium point.

The occurrence of a flip bifurcation indicates a qualitative change in the dynamical behavior of the system. For parameter values below the critical threshold p^*, the equilibrium point remains locally asymptotically stable and the trajectories converge toward a constant population level. However, once the parameter exceeds this threshold, the equilibrium loses its stability and the system evolves toward a periodic solution.

In this region, the state variables alternate between two distinct values in successive iterations, forming a stable period-two oscillation. From an ecological perspective, this transition suggests that predator and prey populations no longer stabilize at a fixed equilibrium density but instead exhibit periodic fluctuations across generations.

Furthermore, the presence of a flip bifurcation may signal the onset of increasingly complex dynamics. As the bifurcation parameter continues to vary, the system may experience successive period-doubling bifurcations, generating cycles with higher periods. This sequence, often referred to as a period-doubling cascade, may ultimately lead to chaotic dynamics characterized by irregular and highly sensitive population fluctuations.

A flip bifurcation occurs when one eigenvalue of the Jacobian matrix E_4 crosses the unit circle through -1, while the other eigenvalue is distinct from both 1 and -1. In order to analyze the flip bifurcation of system (1.3) at its unique positive equilibrium point E_4, we consider δ as the bifurcation parameter. The discriminant of the characteristic equation at equilibrim point E_4 for $\delta = \delta_1 = \dfrac{2}{b_2}$ is

$$\frac{4\left(a_2 b_2^2 f + a_3^2 (h - b_1 + b_2) + a_3 b_2 (a_2 + f (b_2 + h))\right)^2}{a_3^2 b_2^2 (a_3 + b_2 f)} > 0. \tag{3.3}$$

Then, let λ_1 and λ_2 be distinct real roots. Then, we get

$$\lambda = -1, \qquad \lambda_2 = \frac{b_1a_3^2 - (a_3 + b_2f)(b_2a_2 + ha_3 - 2a_3b_2)}{b_1a_3^2 - (a_3 + b_2f)(b_2a_2 + ha_3)}. \tag{3.4}$$

Moreover, $|\lambda_2| \neq 1$ under the following conditions:

$$\frac{a_2b_2a_3 + a_1b_2^2f + 2a_3^2b_2 + ha_3^2 - b_1a_3^2 + 2a_3b_2^2f + hfb_2a_3}{-b_1a_3^2 + a_1b_2a_3 + a_1b_2^2f + ha_3^2 + hfb_2a_3} \neq 1, \tag{3.5}$$

and

$$-b_1a_3^2 + a_1b_2a_3 + a_1b_2^2f + ha_3^2 + hfb_2a_3 \neq 0. \tag{3.6}$$

Note that the eigenvalue analysis shows that the positive equilibrium loses stability only through a real eigenvalue crossing -1. Therefore, the relevant local bifurcation for the our model is the flip bifurcation, whereas the conditions for a Neimark–Sacker bifurcation are not satisfied.

Let us consider the term Ω_{FB} as follows:

$$\Omega_{FB} = \left\{(a_1, a_2, a_3, b_1, b_2, f, h, \delta) \in \mathbb{R}_+^8 : \delta = \frac{2}{b_2} \text{ and the conditions (3.3) – (3.6) hold}\right\}. \tag{3.7}$$

Then, for $(a_1, a_2, a_3, b_1, b_2, f, h, \delta) \in \Omega_{FB}$, system (1.3) can be expressed by

$$\begin{bmatrix} X \\ Y \end{bmatrix} \to \begin{bmatrix} X + \delta\left(\dfrac{X(b_1 - a_1X)}{1 + fY} - a_2XY - hX\right) \\ Y + \delta Y(b_2 - a_3Y) \end{bmatrix}. \tag{3.8}$$

Let $\tilde{\delta}_1$ be a sufficiently small bifurcation parameter satisfying $|\tilde{\delta}_1| \ll 1$. The associated perturbed form of the mapping in (3.8) can then be expressed as follows:

$$\begin{bmatrix} X \\ Y \end{bmatrix} \to \begin{bmatrix} X + (\delta + \tilde{\delta}_1)\left(\dfrac{X(b_1 - a_1X)}{1 + fY} - a_2XY - hX\right) \\ Y + Y(\delta + \tilde{\delta}_1)(b_2 - a_3Y) \end{bmatrix}. \tag{3.9}$$

Now, we apply the transformations

$$x = X - \frac{b_1a_3^2 - a_2a_3b_2 - a_2b_2^2f - ha_3^2 - hfa_3b_2}{a_1a_3^2}, \tag{3.10}$$

$$y = Y - \frac{b_2}{a_3}. \tag{3.11}$$

Then, from the map (3.9), we get

$$\begin{bmatrix} x \\ y \end{bmatrix} \to \begin{bmatrix} a_{11} & a_{12} \\ a_{21} & a_{22} \end{bmatrix}\begin{bmatrix} x \\ y \end{bmatrix} + \begin{bmatrix} g_1(x, y, \tilde{\delta}_1) \\ g_2(x, y, \tilde{\delta}_1) \end{bmatrix}, \tag{3.12}$$

where we have defined

$$\begin{aligned} g_1(x, y, \tilde{\delta}_1) =& a_{13}y^2 + a_{14}x^2 + a_{15}xy + d_{11}x^2\delta_1 + d_{12}xy\delta_1 + d_{13}y^2\delta_1 \\ &+ d_{14}x\delta_1 + d_{15}y\delta_1 + O\left((|x| + |y| + |\delta_1|)^3\right), \end{aligned} \tag{3.13}$$

$$g_2(x, y, \tilde{\delta}_1) = a_{23}y^2 + d_{21}y^2\delta_1 + d_{22}y\delta_1 + O\left((|x| + |y| + |\delta_1|)^3\right), \tag{3.14}$$

and

$$a_{11} = 1 + \frac{(a_2\, b_2^2 f + a_3^2(h - b_1) + a_3\, b_2(a_2 + f\, h))\delta}{a_3(a_3 + b_2 f)}, \tag{3.15}$$

$$a_{12} = \frac{(a_2(a_3 + 2b_2 f) + a_3 f\, h)(a_2\, b_2^2 f + a_3^2(h - b_1) + a_3 b_2(a_2 + f\, h))\delta}{a_1 a_3^2(a_3 + b_2 f)}, \tag{3.16}$$

$$a_{21} = 0, \quad a_{22} = 1 - b_2\, \delta, \tag{3.17}$$

$$a_{13} = -\frac{f^2\delta\,(a_2\, b_2 + a_3\, h)\left(a_2\, b_2^2 f + a_3^2(h - b_1) + a_3\, b_2(a_2 + f\, h)\right)}{a_1 a_3\,(a_3 + b_2 f)^2}, \tag{3.18}$$

$$a_{14} = -\frac{a_1\, a_3\, \delta}{a_3 + b_2 f}, \tag{3.19}$$

$$a_{15} = \frac{(\,-a_2(a_3^2 + 4a_3\, b_2 f + 3b_2^2 f^2) + a_3 f(a_3(b_1 - 2h) - 2b_2 f\, h))\delta}{(a_3 + b_2 f)^2}, \tag{3.20}$$

$$a_{23} = -a_3\delta, \tag{3.21}$$

$$d_{11} = -\frac{a_1\, a_3}{a_3 + b_2 f}, \tag{3.22}$$

$$d_{12} = \frac{-a_2(a_3^2 + 4a_3\, b_2 f + 3b_2^2 f^2) + a_3 f(a_3(b_1 - 2h) - 2b_2 f\, h)}{(a_3 + b_2 f)^2}, \tag{3.23}$$

$$d_{13} = -\frac{f^2\,(a_2\, b_2 + a_3\, h)\left(a_2\, b_2^2 f + a_3^2(h - b_1) + a_3\, b_2(a_2 + f\, h)\right)}{a_1 a_3\,(a_3 + b_2 f)^2}, \tag{3.24}$$

$$d_{14} = \frac{(a_2\, b_2^2 f + a_3^2(h - b_1) + a_3\, b_2(a_2 + f\, h))}{a_3(a_3 + b_2 f)}, \tag{3.25}$$

$$d_{15} = \frac{(a_2(a_3 + 2b_2 f) + a_3 f\, h)(a_2\, b_2^2 f + a_3^2(h - b_1) + a_3 b_2(a_2 + f\, h))}{a_1 a_3^2(a_3 + b_2 f)}, \tag{3.26}$$

$$d_{21} = -a_3, \quad d_{22} = -b_2. \tag{3.27}$$

To transform the coefficient matrix in map (3.12) into its normal form, we apply the following change of variables:

$$\begin{bmatrix} x \\ y \end{bmatrix} = T \begin{bmatrix} u \\ v \end{bmatrix}, \tag{3.28}$$

where T is an invertible matrix and is given by

$$T = \begin{bmatrix} a_{12} & a_{12} \\ -1 - a_{11} & \lambda_2 - a_{11} \end{bmatrix}. \tag{3.29}$$

From (3.12) and (3.28), we get

$$\begin{bmatrix} u \\ v \end{bmatrix} \to \begin{bmatrix} -1 & 0 \\ 0 & \lambda_2 \end{bmatrix} \begin{bmatrix} u \\ v \end{bmatrix} + \begin{bmatrix} g_3(u, v, \tilde{\delta}_1) \\ g_4(u, v, \tilde{\delta}_1) \end{bmatrix}, \tag{3.30}$$

where

$$g_3(u,v,\tilde{\delta}_1) = -\left(\frac{(a_1-\lambda_2)(a_{14}+d_{11}\delta_1)}{a_2(1+\lambda_2)}\right)x^2 - \left(\frac{(a_1-\lambda_2)(a_{13}+d_{13}\delta_1)}{a_2(1+\lambda_2)} + \frac{a_{23}+d_{21}\delta_1}{1+\lambda_2}\right)y^2$$
$$-\left(\frac{(a_1-\lambda_2)d_{15}\delta_1}{a_2(1+\lambda_2)}\right)x - \left(\frac{(a_1-\lambda_2)d_{14}\delta_1}{a_2(1+\lambda_2)} + \frac{d_{22}\delta_1}{1+\lambda_2}\right)y \tag{3.31}$$
$$-\left(\frac{(a_1-\lambda_2)(a_{15}+d_{12}\delta_1)}{a_2(1+\lambda_2)}\right)xy + O\left((|x|+|y|+|\delta_1|)^3\right),$$

$$g_4(u,v,\tilde{\delta}_1) = \left(\frac{(1+a_1)(a_{14}+d_{11}\delta_1)}{a_2(1+\lambda_2)}\right)x^2 + \left(\frac{(1+a_1)(a_{13}+d_{13}\delta_1)}{a_2(1+\lambda_2)} + \frac{a_{23}+d_{21}\delta_1}{1+\lambda_2}\right)y^2$$
$$+\left(\frac{(1+a_1)d_{15}\delta_1}{a_2(1+\lambda_2)}\right)x + \left(\frac{(1+a_1)d_{14}\delta_1}{a_2(1+\lambda_2)} + \frac{d_{22}\delta_1}{1+\lambda_2}\right)y \tag{3.32}$$
$$+\left(\frac{(1+a_1)(a_{15}+d_{12}\delta_1)}{a_2(1+\lambda_2)}\right)xy + O\left((|x|+|y|+|\delta_1|)^3\right),$$

$$x = a_{12}(u+v), \quad y = -u(1+a_1) + v(\lambda_2 - a_1). \tag{3.33}$$

We now invoke the center manifold theorem. Denote by $W^c(0,0,0)$ the center manifold of (3.30) at the point $(0,0)$ in a small neighborhood of $\tilde{\delta}_1 = 0$. Accordingly, $W^c(0,0,0)$ can be approximated as follows:

$$W^c(0,0,0) = \left\{\left(u,v,\tilde{\delta}_1\right) \in \mathbb{R}^3 : v = m_1u^2 + m_2u\tilde{\delta}_1 + m_3\tilde{\delta}_1^2 + O\left((|u|+|\delta_1|)^3\right)\right\}, \tag{3.34}$$

where we have defined

$$m_1 = \frac{a_2(1+a_1)^2(a_{15}-a_{23}) - a_{13}(1+a_1)^3 - a_2^3a_{24} - a_2^2(a_{14}-a_{25})(1+a_1)}{a_2\lambda_2(1+\lambda_2)}, \tag{3.35}$$

$$m_2 = \frac{d_{14}(1+a_1)^2 - a_2(1+a_1)(d_{15}-d_{24}) - a_2^2\,d_{25}}{a_2(1+2\lambda_2+\lambda_2^2)}, \tag{3.36}$$

$$m_3 = 0. \tag{3.37}$$

Therefore,

$$F : u \to -u + k_1u^2 + k_2\,u\,\delta_1 + k_3\,u^2\,\delta_1 + k_4\,u\,\delta_1^2 + k_5\,u^3 + O\left((|u|+|\delta_1|)^3\right), \tag{3.38}$$

$$k_1 = \frac{a_2(-a_{14}\,a_2 + a_{15}(1+a_1))(a_1-\lambda_2) + (1+a_1)^2\,((\lambda_2-a_1)a_{13} - a_{23}\,a_2)}{a_2(\lambda_2+1)}, \tag{3.39}$$

$$k_2 = \frac{a_1^2\,d_{14} + a_1\,(a_2(d_{22}-d_{15}) + d_{14}(1-\lambda_2)) + a_2(d_{15}\,\lambda_2 + d_{22}) - d_{14}\,\lambda_2}{a_2(\lambda_2+1)}, \tag{3.40}$$

$$k_3 = -\frac{k_{3a}+k_{3b}}{a_2^2(-1+\lambda_2^2)} + \frac{k_{3c}\,k_{3d}}{a_2^2(1+\lambda_2)^2} + \frac{k_{3e}+k_{3f}}{a_2(1+\lambda_2)}, \tag{3.41}$$

$$k_{3a} = (1+a_1)\left((1+a_1)^2a_{13} + a_2(-(1+a_1)a_{15} + a_{14}a_2 + a_{23} + a_1a_{23})\right), \tag{3.42}$$

$$k_{3b} = (a_1-\lambda_2)(a_1d_{14} + a_2(-d_{15}+d_{22}) - d_{14}\lambda_2), \tag{3.43}$$

$$k_{3c} = (1 + a_1)(d_{14} + a_1 d_{14} - a_2\, d_{15} + a_2\, d_{22})(a_1 - \lambda_2), \tag{3.44}$$

$$k_{3d} = -2a_2^2 a_{14} - 2a_1^2 a_{13} + a_{15} a_2 - 2a_2\, a_{23} + 2a_1(a_2(a_{15} - a_{23}) + a_{13}(-1 + \lambda_2)) + 2a_{13}\lambda_2 - a_{15} a_2 \lambda_2, \tag{3.45}$$

$$k_{3e} = -a_1^3 d_{13} + a_1^2(a_2(d_{12} - d_{21}) + d_{13}(-2 + \lambda_2)) + a_2^2 d_{11}\lambda_2 + d_{13}\lambda_2 - a_2(d_{21} + d_{12}\lambda_2), \tag{3.46}$$

$$k_{3f} = -a_1(a_2^2 d_{11} + d_{13} + a_2(2d_{21} + d_{12}(-1 + \lambda_2)) - 2d_{13}\lambda_2), \tag{3.47}$$

$$k_4 = \frac{(1 + a_1)(d_{14} + a_1 d_{14} - a_2\, d_{15} + a_2\, d_{22})(a_1 - \lambda_2)(a_1\, d_{14} + a_2(-d_{15} + d_{22}) - d_{14}\lambda_2)}{a_2^2(1 + \lambda_2)^3}, \tag{3.48}$$

$$k_5 = \frac{k_{5a}\, k_{5b}}{a_2^2(-1 + \lambda_2)(1 + \lambda_2)^2}, \tag{3.49}$$

$$k_{5a} = (1 + a_1)((1 + a_1)^2 a_{13} + a_2(-(1 + a_1)a_{15} + a_{14}a_2 + a_{23} + a_1 a_{23}))(a_1 - \lambda_2), \tag{3.50}$$

$$k_{5b} = 2a_1^2 a_{13} - 2a_1(a_2(a_{15} - a_{23}) + a_{13}(-1 + \lambda_2)) + a_{15} a_2(-1 + \lambda_2) + 2(a_{14}a_2^2 + a_2\, a_{23} - a_{13}\lambda_2). \tag{3.51}$$

Next, we define the following two nonzero real numbers as

$$\begin{aligned} l_1 &= \left(\frac{\partial^2 g_3}{\partial u \partial \delta_1} + \frac{1}{2}\frac{\partial F}{\partial \delta_1}\frac{\partial^2 F}{\partial u^2}\right)\Bigg|_{(0,0)} \\ &= \frac{a_1^2 d_{14} - d_{14}\lambda_2 + a_1(d_{14} + a_2(-d_{15} + d_{22}) - d_{14}\lambda_2) + a_2(d_{22} + d_{15}\lambda_2)}{a_2(1 + \lambda_2)}, \end{aligned} \tag{3.52}$$

$$l_2 = \left(\frac{1}{6}\frac{\partial^3 g_3}{\partial u^3} + \left(\frac{1}{2}\frac{\partial^2 F}{\partial u^2}\right)^2\right)\Bigg|_{(0,0)} = k_1^2 + k_5. \tag{3.53}$$

Therefore, about the flip bifurcation of the system, we provide the following result.

Theorem 3.2. *Assume that $l_2 \neq 0$. Then, system* (1.3) *experiences a flip bifurcation at the unique equilibrium point E_4 as the parameter δ varies within a small neighborhood of δ_1. Moreover, if $l_2 > 0$, the period-two solutions emerging from the positive fixed point E_4 are stable; whereas if $l_2 < 0$, the bifurcating period-two solutions are unstable.*

4. Chaos control

In discrete-time systems chaos control is interesting field for lots of researchers and applicable methods used in many topics such as cardiology, communications turbulence, and physics laboratories. In discrete-time models, chaos control can be obtained by using lots of methods and one of them is, state feedback control one OGY [24].

In this section, we investigate OGY feedback control method for chaos. Consider the following controlled system corresponding to (1.3):

$$\begin{aligned} x_{n+1} &= x_n + \delta\left(\frac{x_n(b_1 - a_1 x_n)}{1 + f y_n} - a_2 x_n y_n - h x_n\right) = f(x_n, y_n, b_2), \\ y_{n+1} &= y_n + \delta y_n(b_2 - a_3 y_n) = g(x_n, y_n, b_2), \end{aligned} \tag{4.1}$$

with b_2 chaos control parameter. Furthermore, suppose that for $\varepsilon > 0$, $|b_2 - b_0| < \varepsilon$, and b_0 is the nominal parameter lies at our chaotic regions. Next, suppose that (X^*, Y^*) is an interior unstable

equilibrium point of model (1.3) and is located in some chaotic regions. In order to move the unstable equilibrium point to the stable one, model (1.3) is linearized in the neighborhood of the unstable equilibrium point (X^*, Y^*) as follows:

$$\begin{bmatrix} x_{n+1} - X^* \\ y_{n+1} - Y^* \end{bmatrix} \approx J \begin{bmatrix} x_n - X^* \\ y_n - Y^* \end{bmatrix} + B\left[b_2 - b_0\right], \tag{4.2}$$

where we have defined

$$B = \begin{bmatrix} \frac{\partial f(x_n, y_n, b_0)}{\partial b_0} \\ \frac{\partial g(x_n, y_n, b_0)}{\partial b_0} \end{bmatrix} = \begin{bmatrix} 0 \\ \dfrac{\delta b_2}{a_3} \end{bmatrix}, \tag{4.3}$$

and

$$J = \begin{bmatrix} \frac{\partial f(x_n, y_n, b_0)}{\partial x_n} & \frac{\partial f(x_n, y_n, b_0)}{\partial y_n} \\ \frac{\partial g(x_n, y_n, b_0)}{\partial x_n} & \frac{\partial g(x_n, y_n, b_0)}{\partial y_n} \end{bmatrix} = \begin{bmatrix} J_{11} & J_{12} \\ J_{21} & J_{22} \end{bmatrix}, \tag{4.4}$$

where

$$J_{11} := 1 - \delta \frac{a_3^2 b_1 - (a_3 + b_2 f)(a_2 b_2 + a_3 h)}{a_3 (a_3 + b_2 f)}, \tag{4.5}$$

$$J_{12} := \frac{(a_3 f h + a_3 a_2 + 2 a_3 b_2 f)\left[-a_3^2 b_1 + (a_3 + b_2 f)(a_2 b_2 + a_3 h)\right]}{a_1 a_3^2 (a_3 + b_2 f)}, \tag{4.6}$$

$$J_{21} := 0, \quad J_{22} := 1 - \delta b_2.$$

Then, we denote controllability matrix for system (4.2) as follows:

$$C = [B : JB] = \begin{bmatrix} 0 & \delta^2 b_2 \dfrac{(a_3 f h + a_3 a_2 + 2 a_2 b_2 f)\left(b_1 a_3^2 - a_2 a_3 b_2 - a_2 b_2^2 f - a_3^2 h + b_2 a_3 h\right)}{a_3^3 a_1 (a_3 + b_2 f)} \\ \dfrac{\delta b_2}{a_3} & \dfrac{(1 - \delta b_2)\delta b_2}{a_3} \end{bmatrix}. \tag{4.7}$$

Next, we can see that rank of C is 2. So assume that

$$[b_2 - b_0] = -K \begin{bmatrix} x_n - X^* \\ y_n - Y^* \end{bmatrix}. \tag{4.8}$$

Here, $K = [p_1 \ p_2]$, then system (4.2) can be given as

$$\begin{bmatrix} x_{n+1} - X^* \\ y_{n+1} - Y^* \end{bmatrix} \approx [J - BK] \begin{bmatrix} x_n - X^* \\ y_n - Y^* \end{bmatrix}. \tag{4.9}$$

Moreover, the equilibrium point (X^*, Y^*) is locally asymptotically stable if and only if all eigenvalues of the matrix $J - BK$ are contained within the open unit disk. The Jacobian matrix $J - BK$ corresponding to the controlled system (4.9) is given by

$$J - BK = \begin{bmatrix} 2 + J_{11} & \delta J_{12} \\ -\dfrac{\delta b_2}{a_3} p_1 & 1 - \delta b_2 - \dfrac{\delta b_2}{a_3} \end{bmatrix}, \tag{4.10}$$

where we recall that J_{11} and J_{12} are the quantities defined in (4.5) and (4.6), respectively. The characteristic equation of the Jacobian matrix $J - BK$ is given as follows:

$$P(\lambda) = \lambda^2 - tr[J - BK]\lambda + \det[J - BK] = 0. \tag{4.11}$$

Assume that the characteristic equation (4.11) has eigenvalues λ_1 and λ_2. Then, we obtain

$$\lambda_1 + \lambda_2 = 2 + \delta\frac{a_3^2 b_1 - (a_3 + b_2 f)(a_2 b_2 + a_3 h)}{a_3(a_3 + b_2 f)} - \delta b_2 - \frac{\delta b_2}{a_3} p_2, \tag{4.12}$$

and

$$\begin{aligned}\lambda_1\lambda_2 = \ & \delta^2 b_2 \frac{(a_3 f h + a_3 a_2 + 2a_3 b_2 f)\left[-a_3^2 b_1 + (a_3 + b_2 f)(a_2 b_2 + a_3 h)\right]}{a_1 a_3^3 (a_3 + b_2 f)} p_1 \\ & - \frac{\delta b_2}{a_3}\left(1 + \delta\frac{a_3^2 b_1 - (a_3 + b_2 f)(a_2 b_2 + a_3 h)}{a_3(a_3 + b_2 f)}\right) p_2 \\ & + \left(1 + \delta\frac{a_3^2 b_1 - (a_3 + b_2 f)(a_2 b_2 + a_3 h)}{a_3(a_3 + b_2 f)}\right)(1 - \delta b_2).\end{aligned} \tag{4.13}$$

Next, we must solve the equations $\lambda_1 = \pm 1$ and $\lambda_1\lambda_2 = 1$ to get the lines of marginal stability. These restrictions make sure that $|\lambda_1| < 1$ and $|\lambda_2| < 1$. From $\lambda_1\lambda_2 = 1$ in Eq (4.13), then

$$\begin{aligned}L_1 = & \frac{\left[b_2(a_2(a_3 + 2b_2 f) + a_3 f h)\left(-a_3^2 b_1 + (a_3 + b_2 f)(a_2 b_2 + a_3 h)\right)\right]}{a_1 a_3^3 (a_3 + b_2 f)}\delta^2 p_1 \\ & + \frac{a_1 a_3\left[-a_3(a_3 + b_2 f) + b_1 a_3^2\delta - (a_3 + b_2 f)(a_2 b_2 + a_3 h)\delta\right](-a_3 + b_2(a_3 + p_2))\delta}{a_1 a_3^3 (a_3 + b_2 f)} \\ = & \ 0.\end{aligned}$$

Furthermore, assume that $\lambda_1 = 1$. Then, we obtain the following line for marginal stability:

$$L_2 = \left[\frac{(-1 + p_2)}{a_3} + \frac{b_2(a_2(a_3 + 2b_2 f) + a_3 f h)\left(-a_3^2 b_1 + (a_3 + b_2 f)(a_2 b_2 + a_3 h)\right)}{a_1 a_3^3 (a_3 + b_2 f)}\right] b_2\delta = 0.$$

Lastly, suppose that $\lambda_1 = -1$, then

$$\begin{aligned}L_3 = & 4 + \left[\frac{b_2(a_2(a_3 + 2b_2 f) + a_3 f h)\left(-a_3^2 b_1 + (a_3 + b_2 f)(a_2 b_2 + a_3 h)\right)}{a_1 a_3^3 (a_3 + b_2 f)}\right] b_2\delta^2 \\ & + \left(-\frac{2b_1 a_3}{a_3 + b_2 f} + 2h - \frac{b_2(1 - 2a_2 + 2a_3 + p_2)}{a_3}\right) = 0.\end{aligned} \tag{4.14}$$

In this case, for specific parameter values, the stable eigenvalues are located inside the triangular domain of the $p_1\, p_2$-plane delimited by the lines L_1, L_2, L_3.

5. Numerical examples

In this section, the theoretical findings are supported through numerical simulations performed using Maple 2021 and MATLAB R2024b. The dynamical behavior of the model is investigated under different parameter configurations, and corresponding graphical results are presented for each scenario. While analytical approaches provide exact results, they are often restricted to simplified formulations; in contrast, numerical methods enable a more comprehensive exploration of complex ecological dynamics. It should be emphasized that the parameter values adopted in this study are not derived from experimental or field data, but are selected to illustrate the qualitative behavior of the model.

5.1. Stability and flip bifurcation analysis varying δ.

Assume that the parameter set is chosen as

$$(a_1, a_2, a_3, b_1, b_2, f, h) = (20, 10, 10, 20, 10, 0.01, 0.01),$$

with the initial condition $(x_0, y_0) = (0.45, 0.98)$. For these parameter values, model (1.2) admits a unique positive equilibrium point $E_4 = (0.4944950000, 1)$. The local stability analysis shows that E_4 remains asymptotically stable for $\delta < 0.2$, indicating that the equilibrium behaves as a sink in this parameter region. As the bifurcation parameter δ approaches the critical value $\delta_c = 0.2$, the system experiences a qualitative change in its dynamical behavior. At $\delta = 0.2$, the characteristic equation of the Jacobian matrix evaluated at (E_4) is obtained as

$$\lambda^2 + 1.95839604\lambda + 0.95839604 = 0.$$

The corresponding eigenvalues are $\lambda_1 = -1, \quad \lambda_2 = -0.95839604$, where $\lambda_2| \neq 1$. Since one eigenvalue crosses the unit circle through -1, the conditions for a flip bifurcation are satisfied. Consequently, the positive equilibrium point E_4 undergoes a flip bifurcation at the critical value $\delta = 0.2$.

The bifurcation structures illustrated in Figure 3(a) and (b), together with the maximum Lyapunov exponent (MLE) profile shown in Figure 3(c), provide further insight into the system's dynamics. In particular, positive MLE values confirm the emergence of chaotic behavior. It is evident from the bifurcation diagrams that the equilibrium E_4 loses stability at $\delta = 0.2$, which is consistent with the onset of a flip bifurcation. Furthermore, the phase portraits presented in Figure 4 support this transition, revealing a cascade toward chaos.

From an ecological perspective, the transition to chaos implies that even minor variations in environmental conditions or parameter values may lead to significant and unpredictable fluctuations in population densities. Such sensitivity can manifest as irregular oscillatory patterns, abrupt population declines, or sudden outbreaks. Conversely, parameter regimes associated with stability correspond to more regular predator-prey interactions, such as periodic oscillations or steady coexistence states, which are generally indicative of a resilient ecological system.

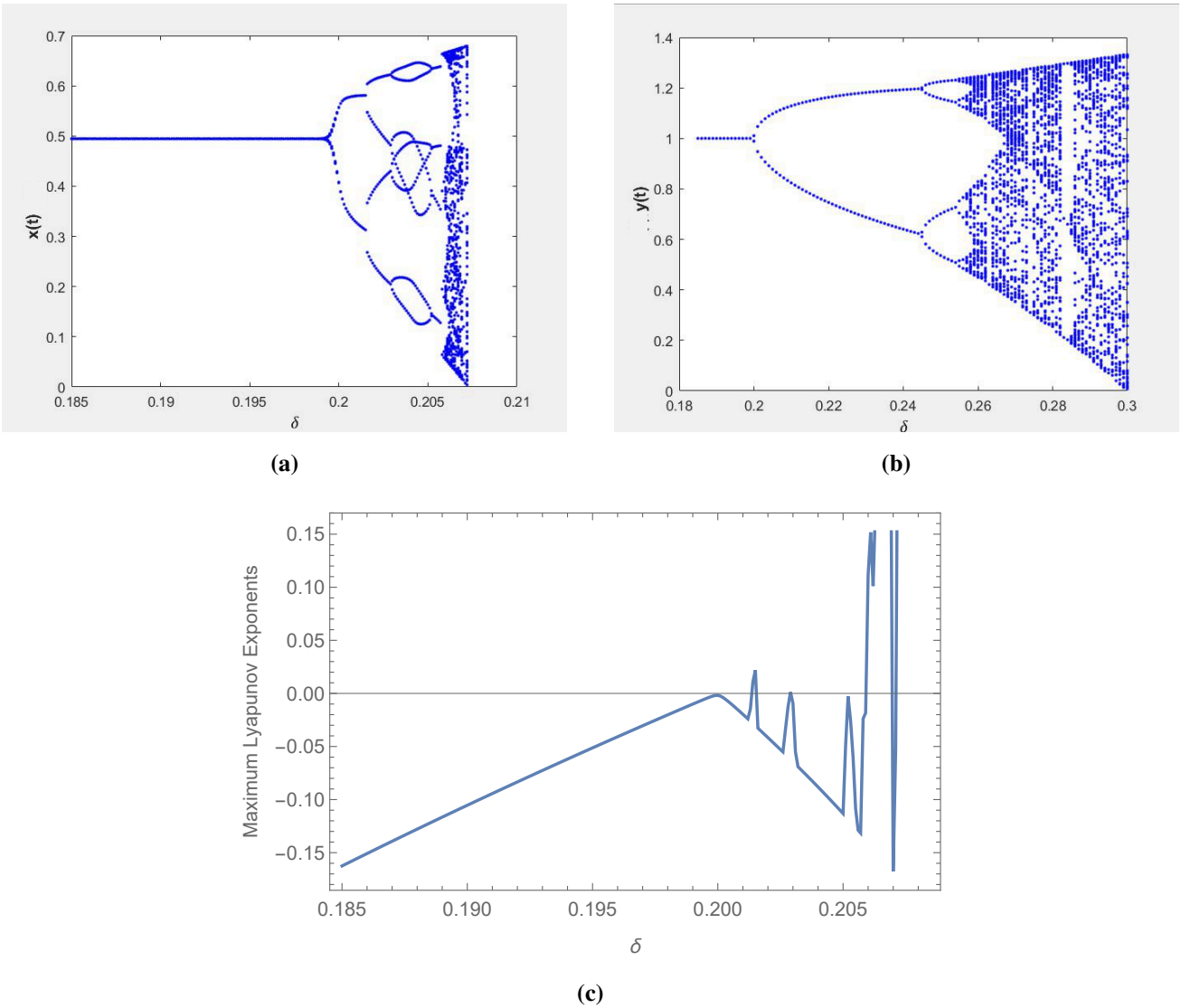

(a) **(b)**

(c)

Figure 3. Dynamical behavior of system (1.3) for $(a_1, a_2, a_3, b_1, b_2, f, h) = (20, 10, 10, 20, 10, 0.01, 0.01)$. The subfigures (a) and (b) present the bifurcation diagrams, subfigure (c) shows the corresponding MLE. Together, these plots illustrate the transitions between different dynamical regimes as the bifurcation parameter varies.

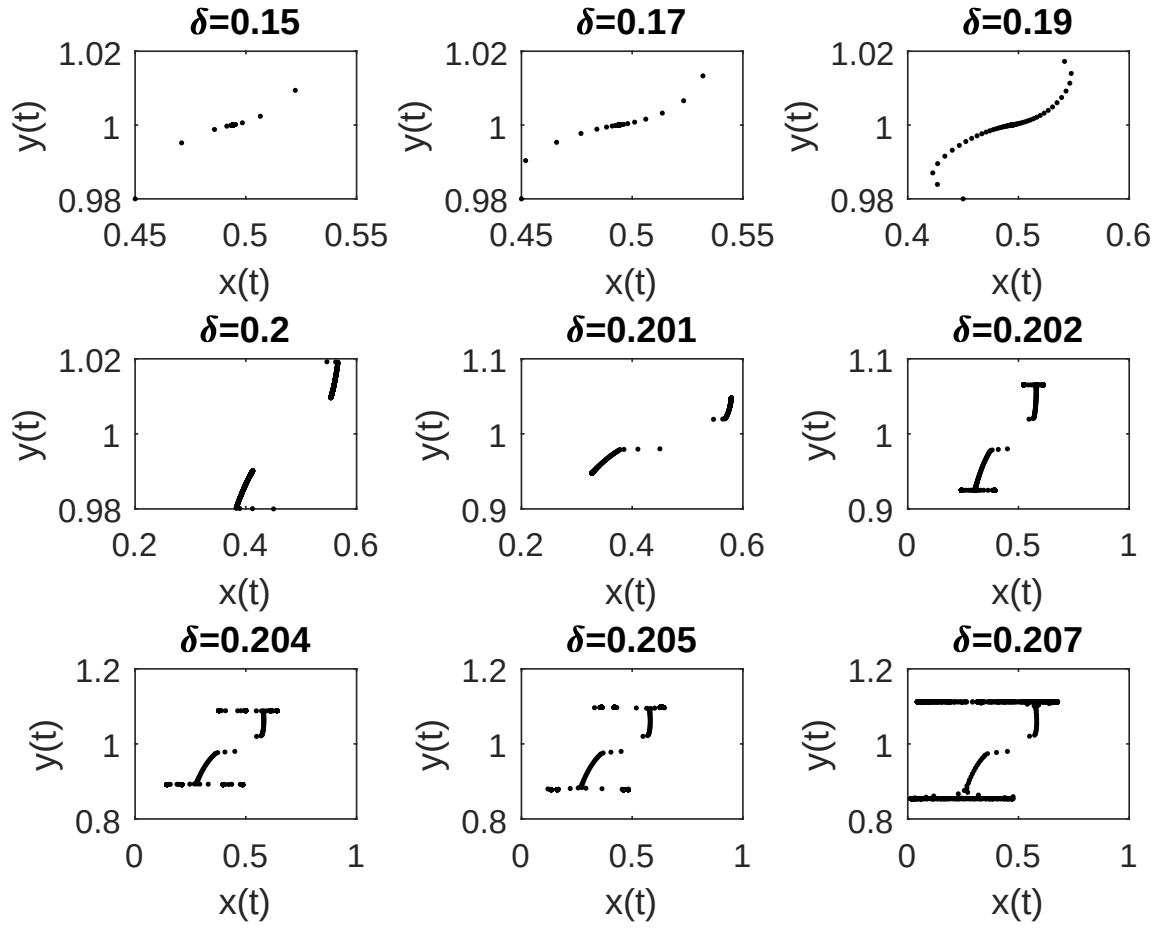

Figure 4. Phase portraits for flip bifurcation for different values of δ.

The following stage is devoted to the application of the OGY control method to regulate the chaotic dynamics generated by period-doubling bifurcation behavior. To implement the OGY feedback control approach for system (1.3), the parameter set is selected as

$$(a_1, a_2, a_3, b_1, b_2, f, h, \delta) = (20, 10, 10, 20, 10.46, 0.01, 0.01, 0.2)\,.$$

Under these parameter values, system (1.3) admits the unstable equilibrium point $(0.4710241900, 1)$. Since this equilibrium state loses stability, it is considered as the desired operating point in the control procedure. Therefore, the corresponding controlled form of the system can be expressed as follows:

$$\begin{aligned} x_{n+1} &= (0.998)\, x_n + \frac{(0.2)\, x_n(-20x_n + 20)}{(0.01)\, y_n + 1} - 2x_n y_n, \\ y_{n+1} &= y_n + (0.2)\, y_n(-10y_n + 10.46). \end{aligned} \tag{5.1}$$

We have

$$A = \begin{bmatrix} -0.864593116 & -0.9518095250 \\ 0 & -1.092 \end{bmatrix},$$

$$B = \begin{bmatrix} 0 \\ 0.2092000000 \end{bmatrix},$$

and

$$\begin{aligned} C &= \begin{bmatrix} B : AB \end{bmatrix} \\ &= \begin{bmatrix} 0 & -0.1991185526 \\ 0.2092000000 & -0.2284464000 \end{bmatrix}. \end{aligned}$$

Next, it is easy to see that the rank of the C matrix is 2. Thus, system (5.1) is controllable. Then, the Jacobian matrix $A - BK$ of the controlled system (5.1) is given by

$$A - BK = \begin{bmatrix} -0.864593116 & -0.9518095250 \\ -0.2092p_1 & -1.092 - 0.2092p_2 \end{bmatrix}.$$

Moreover, the lines L_1, L_2, and L_3 for marginal stability are given by

$$\begin{aligned} L_1 &= -0.1991185527p_1 + 0.1808728799p_2 - 0.055864318 = 0, \\ L_2 &= -0.1991185527p_1 + 0.390072879p_2 + 3.900728798 = 0, \\ &\text{and} \\ L_3 &= -0.1991185526p_1 - 0.0283271202p_2 - 0.012457434 = 0. \end{aligned}$$

Then, the stable triangular region bounded by marginal lines L_1, L_2, and L_3 for the controlled system (5.1) is shown in Figure 5.

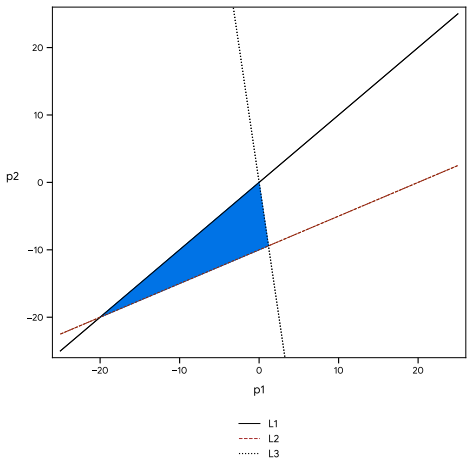

Figure 5. Triangular stability region bounded by L_1, L_2, and L_3 for the controlled system (5.1).

5.2. *Stability and flip bifurcation analysis varying f.*

At $(a_1, a_2, a_3, b_1, b_2, h, \delta) = (0.8, 2.5, 2, 2.425, 0.6, 0.44, 3.333333334)$, model (1.3) has the unique positive equilibrium point $(1.00825, 0.3)$. Furthermore, the characteristic equation of the Jacobian matrix of system (1.3) is a follows:

$$\lambda^2 + 1.508\lambda + 0.508.$$

The eigenvalues are obtained as $\lambda_1 = -1$ and $\lambda_2 = -0.508$ with $|\lambda_2| \neq 1$. The bifurcation diagram of model (1.3) is given in Figure 6(a).

The numerical investigation reveals that the fear effect constitutes an important mechanism governing the qualitative dynamics of the system. Variation of the control parameter f leads to a sequence of bifurcations and a transition from regular to chaotic behavior. As f decreases, a critical transition is observed near $f = 1.2$, where a flip bifurcation occurs. This bifurcation marks the onset of oscillatory dynamics. Further reduction in f induces a cascade of successive period-doubling bifurcations, ultimately leading to chaotic dynamics for $f < 1.2$.

The focus is now on examining the effect of fear on prey and predator populations in the stable region. The time-dependent changes in prey and predator population densities under different fear values are presented in Figure 6(b) and (c). The numerical results show that an increase in fear intensity leads to a significant decrease in prey population density and accelerates the system's convergence to equilibrium. This behavior demonstrates that the fear effect introduces a damping mechanism into the system, thereby reducing oscillations and facilitating faster convergence to equilibrium. In contrast, the predator population exhibits only a weak sensitivity to changes in the fear parameter.

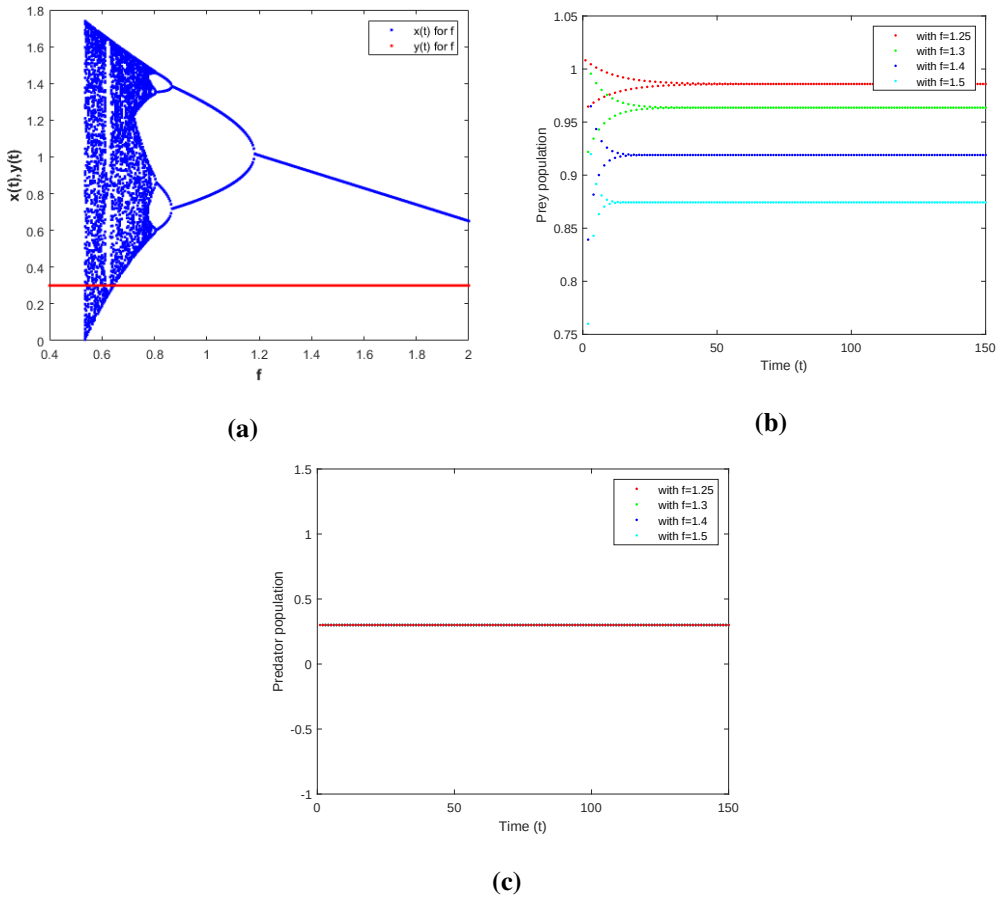

Figure 6. The subfigure (a) shows bifurcation diagram x_t, y_t for the fear effect, and subfigures (b) and (c) show the population densities of prey and predator, respectively, species under different fear effects.

5.3. Stability and flip bifurcation analysis varying h.

Assume that $(a_1, a_2, a_3, b_1, b_2, f, \delta) = (0.8, 2.5, 2, 2.425, 0.6, 1.2, 3.333333334)$. Under these parameter values, model (1.3) admits a unique positive equilibrium point given by $(1.00825, 0.3)$. Taking the harvesting parameter $h \in [0.2, 0.55]$ as the bifurcation parameter, the system exhibits a flip bifurcation around the critical value $h \approx 0.44$. As illustrated in Figure 7(a), the stable equilibrium loses its stability near this threshold, giving rise to periodic oscillations through a period-doubling mechanism. Moreover, decreasing the harvesting parameter beyond this critical point generates a sequence of additional period-doubling bifurcations, indicating a progressive transition from regular oscillatory behavior to chaotic dynamics when $h < 0.44$.

The identical predator trajectories in Figures 6(c) and 7(c) are expected since the predator dynamics are independent of the fear and harvesting parameters in the proposed model. Consequently, varying these parameters does not alter the predator population trajectory.

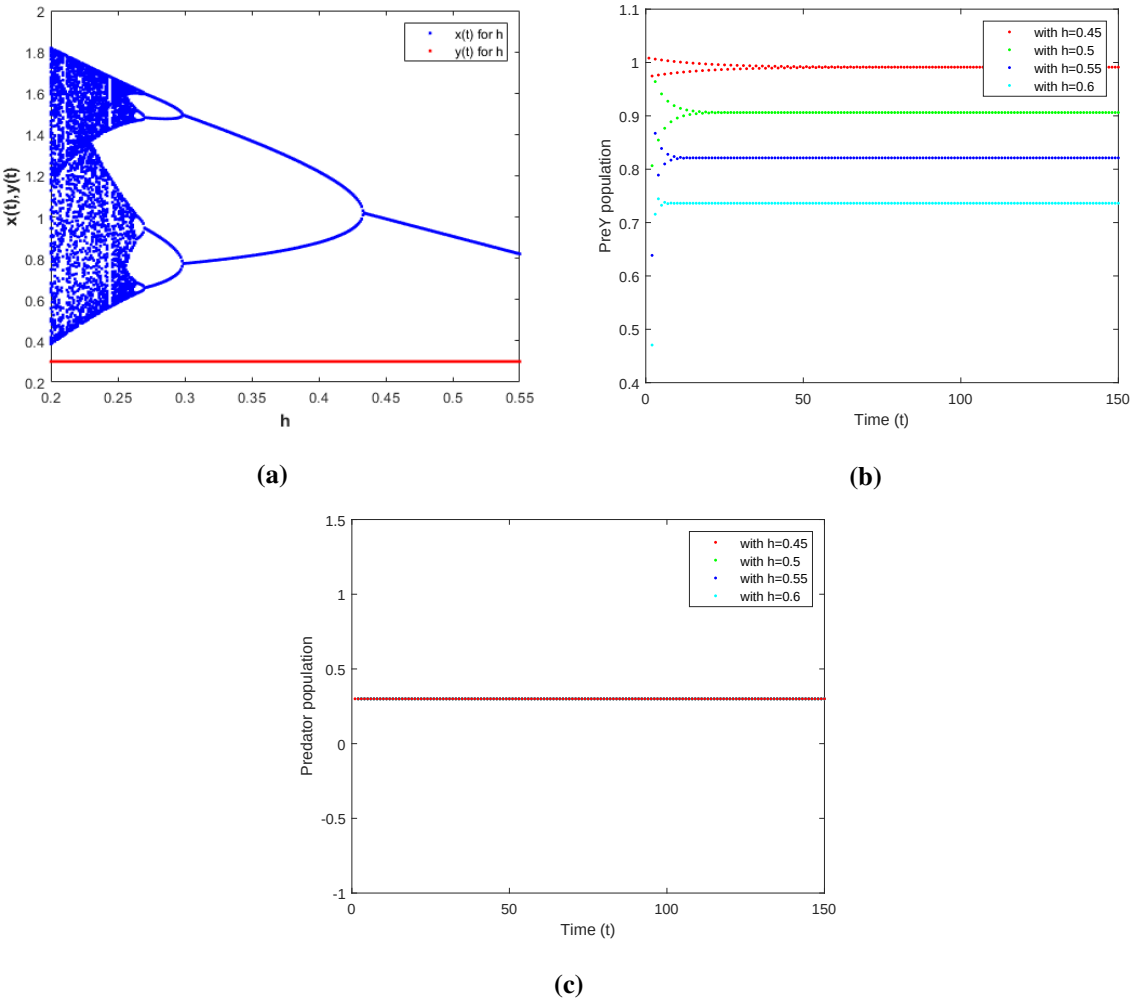

Figure 7. Subfigure (a) shows the bifurcation diagram x_t, y_t for the harvesting effect, and subfigures (b) and (c) show the population densities of prey and predator, respectively, species under different harvesting effects.

The effect of the harvest rate on the densities of the prey and predator populations was examined in the steady-state region. The time-dependent changes in the prey and predator populations for different values of the harvest rate are shown in Figure 7(b) and (c). Figure 7(b) shows that as the harvest rate h increases, the prey population density decreases significantly, and the system reaches its equilibrium state more quickly. This indicates that harvest pressure imposes an additional mortality effect on the prey population, thereby limiting its size. Additionally, it is observed that the increasing harvest effect suppresses fluctuations in the system, making the dynamics more stable.

However, Figure 7(c) shows that, despite the increase in the harvesting parameter, there was no significant change in the predator population density. This result indicates that, within the examined parameter range, the predator population continues to have access to sufficient food resources to sustain the current prey density, and from a biological perspective the harvest effect does not have a direct, noticeable impact on predator dynamics. The predator population exhibits a certain degree of resistance or tolerance to this change.

6. Conclusions

In this study, a discrete-time predator-prey model incorporating the fear effect and harvesting mechanisms was examined. The developed model provides a biologically more realistic representation of ecological interactions by simultaneously accounting for the behavioral response of the prey species to the presence of predators and the impact of human-induced harvesting activities on population dynamics.

As part of the systematic analysis, the existence of equilibrium points was first determined, and their topological classifications were given. In this context, the local stability conditions of the coexistence equilibrium were analyzed in detail. Subsequently, the step size parameter was treated as a bifurcation parameter; using center manifold theory and normal form analysis, it was theoretically demonstrated that the positive equilibrium undergoes a flip bifurcation under appropriate conditions. Both analytical and numerical findings indicate that the system can transition from a stable equilibrium state to periodic oscillations and more complex dynamic states. Furthermore, the chaotic dynamics arising from the flip bifurcation were successfully stabilized using the OGY feedback control method. Through appropriate parameter selection, instability in the system was eliminated, the population was returned to a stable equilibrium state, and it was thus demonstrated that chaotic behavior can be effectively controlled. The results indicate that increasing levels of fear and harvest reduce prey population density, whereas the predator population is less affected by these changes. Overall, the findings confirm the decisive role of fear effects and harvest processes in the long-term dynamics of discrete-time predator-prey interactions. The proposed model and analytical approach provide a deep understanding of the effects of indirect ecological impacts and human interventions on stability, bifurcation, and chaos. These results provide important insights for ecological management and conservation strategies, particularly in ecosystems where population data are collected at discrete time intervals. Future studies are expected to incorporate factors such as time lags, the Allee effect, seasonality, and environmental noise into the model to achieve a more comprehensive ecological framework.

Author contributions

Figen Kangalgil, Nilufer Topsakal, and Mehmet Unlu: Conceptualization, methodology, investigation, writing original draft. All authors have read and approved the final version of the manuscript for publication.

Use of Generative-AI tools declaration

The authors declare they have not used Artificial Intelligence (AI) tools in the creation of this article.

Acknowledgments

This study has been supported by the Recep Tayyip Erdoğan University Development Foundation (Grant number: 02026003018193). In addition, this work was supported by the Recep Tayyip Erdoğan University Research Fund as part of the Scientific Research Project under project number FBA–2025–2273.

Conflict of interest

The authors declare no conflict of interest.

References

1. W. B. Cannon, *Bodily changes in pain, hunger, fear, and rage: An account of recent researches into the function of emotional excitement*, D. Appleton & Company, 1915. https://doi.org/10.1037/10013-000
2. X. Wang, L. Zanette, X. Zou, Modeling the fear effect in predator-prey interactions, *J. Math. Biol.*, **73** (2016), 1179–1204. https://doi.org/10.1007/s00285-016-0989-1
3. X. Wang, X. Zou, Modeling the fear effect in predator-prey interactions with adaptive avoidance of predators, *Bull. Math. Biol.*, **79** (2017), 1325–1359. https://doi.org/10.1007/s11538-017-0287-0
4. P. Panday, N. Pal, S. Samanta, J. Chattopadhyay, A three species food chain model with fear induced trophic cascade, *Int. J. Appl. Comput. Math.*, **5** (2019), 100. https://doi.org/10.1007/s40819-019-0688-x
5. H. Zhang, Y. Cai, S. Fu, W. Wang, Impact of the fear effect in a prey-predator model incorporating a prey refuge, *Appl. Math. Comput.*, **356** (2019), 328–337. https://doi.org/10.1016/j.amc.2019.03.034
6. P. Cong, M. Fan, X. Zou, Dynamics of a three-species food chain model with fear effect, *Commun. Nonlinear Sci. Numer. Simul.*, **99** (2021), 105809. https://doi.org/10.1016/j.cnsns.2021.105809
7. S. Pal, P. K. Tiwari, A. K. Misra, H. Wang, Fear effect in a three-species food chain model with generalist predator, *Math. Biosci. Eng.*, **21** (2024), 1–33. https://doi.org/10.3934/mbe.2024001
8. M. He, Z. Li, Stability of a fear effect predator-prey model with mutual interference or group defense, *J. Biol. Dyn.*, **16** (2022), 480–498. https://doi.org/10.1080/17513758.2022.2091800

9. S. Pal, N. Pal, S. Samanta, J. Chattopadhyay, Effect of hunting cooperation and fear in a predator-prey model, *Ecol. Complex.*, **39** (2019), 100770. https://doi.org/10.1016/j.ecocom.2019.100770
10. J. Liu, P. Lv, B. Liu, T. Zhang, Dynamics of a predator-prey model with fear effect and time delay, *Complexity*, **2021** (2021), 9184193. https://doi.org/10.1155/2021/9184193
11. Y. Tan, Y. Cai, R. Yao, M. Hu, W. Wang, Complex dynamics in an eco-epidemiological model with the cost of anti-predator behaviors, *Nonlinear Dyn.*, **107** (2022), 3127–3141. https://doi.org/10.21203/rs.3.rs-812740/v1
12. Y. Lv, H. Wang, J. Ding, Q. Zhu, Dynamic analysis of a stochastic three species predator-prey model with intraguild predation and predator-switching, *Commun. Nonlinear Sci. Numer. Simul.*, **157** (2026), 109748. https://doi.org/10.1016/j.cnsns.2026.109748
13. G. Dai, M. Tang, Coexistence region and global dynamics of a harvested predator-pray systems, *SIAM J. Appl. Math.*, **58** (1998), 193–210. https://doi.org/10.1137/S003613999427579
14. D. Elmacı, F. Kangalgil, Complex dynamics of a discrete prey-predator model exposing to harvesting and Allee effect on the prey species with chaos control, *Internat. J. Bifur. Chaos*, **30** (2024), 2450114. https://doi.org/10.1142/S0218127424501141
15. A. R. M. Jamil, R. K. Naji, Modeling and analyzing the influence of fear on the harvested modified Leslie–Gower model involving nonlinear prey refuge, *Mathematics*, **10** (2022), 2857. https://doi.org/10.3390/math10162857
16. Y. Chong, Y. Hou, S. Chen, F. Chen, The influence of fear effect to the dynamic behaviors of Lotka–Volterra amensalism model, *Eng. Lett.*, **32** (2024), 1233–1242.
17. T. K. Kar, K. S. Chaudhuri, On non-selective harvesting of a multispecies fishery, *Internat. J. Math. Ed. Sci. Tech.*, **33** (2022), 543–556. https://doi.org/10.1080/00207390210131533
18. X. Song, L. Chen, Optimal harvesting and stability for a two-species competitive system with stage structure, *Math. Biosci.*, **170** (2001), 173–186. https://doi.org/10.1016/s0025-5564(00)00068-7
19. S. Işık, F. Kangalgil, M. J. Uddin, S. M. S. Rana, An investigation of the discrete-time model subject to immigration, harvesting, and Allee effect, *Internat. J. Bifur. Chaos*, **35** (2024), 2550022. https://doi.org/10.1142/S0218127425500221
20. S. Jana, S. Guria, U. Das, T. K. Kar, A. Ghorai, Effect of harvesting and infection on predator in a prey-predator system, *Nonlinear Dyn.*, **81** (2015), 917–930. https://doi.org/10.1007/s11071-015-2040-2
21. S. Işık, A study of stability and bifurcation analysis in discrete-time predator–prey system involving the Allee effect, *Int. J. Biomath.*, **12** (2017), 1950011. https://doi.org/10.1142/S1793524519500116
22. D. Elmacı, F. Kangalgil, Stability, Neimark-Sacker bifurcation analysis of prey-predator model with strong Allee effect and chaos control, *Erzincan Üniv. Fen Bilim. Enst. derg.*, **15** (2022), 775–787. https://doi.org/10.18185/erzifbed.1207680
23. F. Kangalgil, S. Isık, Dynamical complexities in a discrete-time predator-prey system as a consequences of the weak Allee effect on prey, *Miskolc Math. Notes*, **24** (2023), 209–226. https://doi.org/10.18514/MMN.2023.3644

24. E. Ott, C. Grebogi, J. A. Yorke, Controlling chaos, *Phys. Rev. Lett.*, **64** (1990), 1196–1199. https://doi.org/10.1103/PhysRevLett.64.1196
25. F. D. Chen, L. Q. Pu, L. Y. Yang, Positive periodic solution of a discrete obligate Lotka–Volterra model, *Commun. Math. Biol. Neurosci.*, **2015** (2015), 14.
26. X. D. Xie, Z. S. Miao, Y. L. Xue, Positive periodic solution of a discrete Lotka–Volterra commensal symbiosis model, *Commun. Math. Biol. Neurosci.*, **2015** (2015), 2.
27. F. Chen, H. Wu, X. Xie, Global attractivity of a discrete cooperative system incorporating harvesting, *Adv. Differ. Equ.*, **2016** (2016), 268. http://dx.doi.org/10.1186/s13662-016-0996-y
28. P. Georgescu, D. Maxin, H. Zhang, Global stability results for models of commensalism, *Int. J. Biomath.*, **10** (2017), 1750037. https://doi.org/10.1142/S1793524517500371
29. R. Y. Han, F. D. Chen, Global stability of a commensal symbiosis model with feedback controls, *Commun. Math. Biol. Neurosci.*, **2015** (2015), 15.
30. Q. F. Lin, Dynamic behaviors of a commensal symbiosis model with non-monotonic functional response and non-selective harvesting in a partial closure, *Commun. Math. Biol. Neurosci.*, **2018** (2018), 4. https://doi.org/10.28919/cmbn/3652
31. Z. S. Miao, X. D. Xie, L. Q. Pu, Dynamic behaviors of a periodic Lotka–Volterra commensal symbiosis model with impulsive, *Commun. Math. Biol. Neurosci.*, **2015** (2015), 3.
32. R. X. Wu, L. Li, Q. F. Lin, A Holling type commensal symbiosis model involving Allee effect, *Commun. Math. Biol. Neurosci.*, **2018** (2018), 6. https://doi.org/10.28919/cmbn/3679
33. R. X. Wu, L. Lin, X. Y. Zhou, A commensal symbiosis model with Holling type functional response, *J. Math. Comput. Sci.*, **16** (2016), 364–371. http://dx.doi.org/10.22436/jmcs.016.03.06
34. Y. L. Xue, X. D. Xie, F. D. Chen, R. Y. Han, Almost periodic solution of a discrete commensalism system, *Discrete Dyn. Nat. Soc.*, **2015** (2015), 295483. https://doi.org/10.1155/2015/295483
35. K. Yang, Z. Miao, F. Chen, X. Xie, Influence of single feedback control variable on an autonomous Holling-II type cooperative system, *J. Math. Anal. Appl.*, **435** (2016), 874–888. https://doi.org/10.1016/j.jmaa.2015.10.061
36. R. Y. Han, Y. L. Xue, L. Y. Yang, On the existence of positive periodic solution of a Lotka–Volterra amensalism model, *J. Rongyang Univ.*, **33** (2015), 22–26.
37. G. C. Sun, Qualitative analysis on two populations amensalism model, *J. Jiamusi Univ. (Nat. Sci. Ed.)*, **21** (2003), 283–286.
38. R. Wu, A two species amensalism model with non-monotonic functional response, *Commun. Math. Biol. Neurosci.*, **2016** (2016), 19.
39. R. X. Wu, L. Zhao, Q. X. Lin, Stability analysis of a two species amensalism model with Holling II functional response and a cover for the first species, *J. Nonlinear Funct. Anal.*, **2016** (2016), 1–15.
40. R. Wu, Dynamic behaviors of a nonlinear amensalism model, *Adv. Differ. Equ.*, **2018** (2018), 187. https://doi.org/10.1186/s13662-018-1624-9

41. Z. F. Zhu, Q. L. Chen, Mathematical analysis on commensalism Lotka–Volterra model of populations, *J. Jixi Univ.*, **8** (2008), 100–101.

42. F. Chen, Y. Chong, S. Chen, Global stability of a commensal symbiosis model with Holling II functional response and feedback controls, *WSEAS Trans. Syst. Control*, **17** (2022), 279–286. http://dx.doi.org/10.37394/23203.2022.17.32

43. X. Xi, J. N. Griffin, S. Sun, Grasshoppers amensalistically suppress caterpillar performance and enhance plant biomass in an alpine meadow, *Oikos*, **122** (2013), 1049–1057. https://doi.org/10.1111/j.1600-0706.2012.00126.x

AIMS Press